Journal of Magnetic Resonance **146,** 204–219 (2000)
doi:10.1006/jmre.2000.2126, available online at http://www.idealibrary.com on IDEAL®

Spinning-Frequency-Dependent Narrowband RF-Driven Dipolar Recoupling

G. Goobes, G. J. Boender,[1] and S. Vega

Department of Chemical Physics, Weizmann Institute of Science, 76100 Rehovot, Israel

Received March 22, 2000; revised May 18, 2000

Dipolar recoupling techniques of homonuclear spin pairs are commonly used for distance or orientation measurements in solids. Accurate measurements are interfered with by broadening mechanisms. In this publication narrowband RF-driven dipolar recoupling magnetization exchange experiments are performed as a function of the spinning frequency to reduce the effect of zero-quantum T_2 relaxation. To enhance the exchange of magnetization between the coupled spins, a fixed number of rotor-synchronous π-pulses are applied at spinning frequencies approaching the rotational resonance (R^2) conditions. The analysis of the powder averaged dipolar decay curves of the spin magnetizations as a function of the spinning frequency provides a quantitative measure of the dipolar coupling. An effective Hamiltonian for this experiment is derived, taking into account all chemical shift parameters of the spins. The length of the nbRFDR mixing time and the number of rotor cycles per π-pulse are optimized by numerical simulations for sensitive probing of the dipolar coupling strength. The zero-quantum T_2 relaxation time can easily be taken into account in the data analysis, because the overall exchange time is almost constant in these experiments. Spinning-frequency-dependent nbRFDR experiments near the $m = 1$ and $m = 2\,R^2$ condition are shown for doubly ^{13}C-labeled hydroxybutyric acid. © 2000 Academic Press

Key Words: **magic angle spinning; rf-driven dipolar recoupling; distance measurement; rotational resonance; spinning frequency dependence.**

INTRODUCTION

Nuclear dipole–dipole interaction plays an important role in structural investigations by solid-state NMR studies. This spin–spin interaction consists of bilinear terms that are inversely proportional to the cube of the distance between the nuclei. A large variety of radio frequency (rf) schemes have been developed to obtain internuclear distances in static and rotating polycrystalline samples (*1–13*). In the last decade almost all distance measurements have been performed under magic angle spinning (MAS) conditions (*2–13*). MAS averages out the chemical shift anisotropy and the secular dipolar interaction of spin $\frac{1}{2}$ nuclei by producing rotational echoes and consequently narrowing spectral lines (*14*, *15*). The nonsecular flip-flop terms of the homonuclear dipolar interaction between the spins are not averaged out (*15*). Thus MAS rotational echoes of a homonuclear coupled spin system decay according to an effective dipolar interaction that is strongly dependent on the isotropic chemical shift difference between the interacting spins. Matching this chemical shift difference to a multiple integer of the spinning frequency enhances the dipolar decay significantly (*16*) and can be used to determine internuclear distances (*3*, *17*). This rotational resonance (R^2) experiment has been extensively used to obtain valuable structural information for biological molecules (*18*). Increased spin diffusion in natural abundant ^{13}C spins has also been observed at the rotational resonance criteria (*19*).

R^2 experiments on homonuclear spin pairs can be described by a spin evolution in the zero-quantum subspace. A zero-quantum relaxation time must be introduced to represent effects on the spin pair that are not directly correlated to the chemical shift or the dipolar interactions (*3*, *20*). The dipolar decay of the signals during the magnetization exchange R^2 experiment is affected by the chemical shift anisotropy (CSA) interactions of the coupled spins as well. Hence, accurate data analysis of this experiment is fairly complicated.

Other experiments for measuring distances in homonuclear spins have been introduced. In the SEDRA (*5*), RFDR (*6*), and RIL (*9*) experiments the zero-quantum decay is extended beyond the stringent R^2 condition while in other experiments (*4*, *10–12*) the dipolar decay occurs in the double-quantum space where this resonance condition is irrelevant. All experiments use rf irradiation fields in the form of short synchronously applied pulses or phase-modulated continuous wave (CW) irradiation fields. In the latter, the chemical shift influences on the dipolar decays are minimized, while in the pulse recoupling experiments the effect of the chemical shift anisotropy is retained. In the SEDRA and RFDR pulse experiments a set of synchronously applied π pulses on a rotating sample induces dipolar decay of signal. These pulses on coupled spins relieve the strict R^2 condition and broaden the range of spinning frequencies over which dipolar recoupling occurs. The interpretation of the experimental data in these experiments can be somewhat more complicated than in other experiments; however, they do not require intense rf power, are tolerant to pulse imperfections (*21*), and impose no limiting criterion on

[1] Present address: ID-Lelystad, P.O. Box 65, 8200 AB Lelystad, The Netherlands.

1090-7807/00 $35.00

the ratio between the rf power and the spinning rate. Selective polarization exchange between spin pairs is possible via a modified RFDR experiment (*22, 23*). By extending the time between consecutive pulses to integer multiples of the rotor period, $N\tau_R$, instead of one rotor period, the bandwidth of recoupling is narrowed. These narrowband RFDR (nbRFDR) experiments were described both theoretically and experimentally elsewhere (*22, 23*).

All these recoupling techniques still suffer from interference by the zero-quantum (ZQ) relaxation process as in R^2 experiments. Short relaxation times can mask measurements of weak dipolar interactions. Quantifying the ZQ relaxation parameters is not a trivial task, and only lately have experiments been devised to measure the homogeneous and inhomogeneous ZQ broadening in homonuclear spin systems (*20, 25, 26*). New variations of established techniques that are aimed at measurements of the dipolar decay independent of other attenuating factors have emerged recently. Costa and co-workers (*24*) have suggested rotational resonance tickling (R^2T) to recouple the dipolar interaction with reduced dependence on ZQ relaxation. Constant-time homonuclear dipolar recoupling by Bennett *et al.* (*21*) was introduced to enable relaxation-free measurements of dipolar dephasing. Balazs *et al.* have used constant-time R^2 to eliminate variable rf heating at long decoupling times (*27*).

We have used the spinning frequency dependence of the longitudinal exchange in nbRFDR experiments to measure distances and conformations of two nonequivalent ^{13}C nuclei. The experiment is performed without variation of the time or rf fields in order to minimize the effect of the ZQ relaxation mechanism and other experimental factors on the data analysis. The selectivity of the pulse cycle is preserved; therefore, only pairs with chemical shift differences that are in the nbRFDR recoupling bandwidth will exhibit strong magnetization exchange.

In the following, an average Hamiltonian for the nbRFDR experiments is derived, and a relaxation model that takes into account zero-quantum relaxation together with relaxation mechanisms induced by the rf pulses is discussed. A methodology for obtaining internuclear distances from nbRFDR experiments as a function of the spinning frequency is then suggested. Finally, after presenting some details about the materials and the experiments, the results of spinning-frequency-dependent nbRFDR experiments, analyzed in terms of spin–spin distance and relative CSA orientation, are shown.

NARROWBAND RFDR RECOUPLING

The RFDR Experiment

In a one-dimensional RFDR (*6*) experiment on a rotating polycrystalline sample the weak dipolar interaction between two dipolar coupled homonuclear spins, otherwise averaged by MAS, is recovered by means of their chemical shift difference modulated by rf irradiation. The equilibration of the spin magnetizations is induced by the recoupled dipolar interaction. It can be measured as an attenuation of the magnetization difference and analyzed in terms of a nuclear distance. Elucidation of the dipolar coupling strength from the decay of the magnetizations can be complicated by the dependence of the effective interaction on the chemical shift parameters of both spins. However, this fact can also be utilized to obtain additional conformational information. For example, the mutual orientation of the CSA tensors of the spins can be deduced when prior knowledge of the distance separating the spins is available (*21*). RFDR experiments can, therefore, provide structural information about the interacting spins and can be used as an alternative or complementary avenue for the many available techniques used in structural MAS NMR.

The 1D RFDR pulse sequence starts with preparation of the spins in opposite polarizations and is followed by a set of π pulses that are applied synchronously with the rotor cycle. These pulses induce spin exchange that is promoted by the dipolar interaction. The time dependence of the polarization difference is measured by transferring the longitudinal magnetization to observable signals and following their intensities as a function of the length of the dipolar-mixing period. The dependence of the RFDR dipolar recoupling on the isotropic chemical shift difference, $\Delta\omega$, is rather broad and efficient magnetization exchange is expected over a range of frequencies crudely defined by $\omega_R < \Delta\omega < 2\omega_R$, where ω_R is the spinning frequency (*13*). Outside this range, less pronounced exchange is expected around the rotational resonance conditions (*3, 13, 16*), i.e., in the vicinity of $\Delta\omega = 0$ and $\Delta\omega = m\omega_R$ for integer $m \geq 3$. The broadband nature of the recoupling permits observation of exchange between several spin pairs simultaneously. This is advantageous for correlation spectroscopy of multiple spins (*6, 28*), but not for accurate distance measurements (*29*).

The bandwidth of frequencies over which recoupling takes place can be narrowed by extending the number of rotor periods $N\tau_R$ between consecutive π pulses. Boender *et al.* (*24*) and Bennett *et al.* (*23*) have separately shown that such a modification creates frequency-selective exchange that can assist in measuring weak dipolar couplings in the presence of larger dipolar couplings.

The Narrowband RFDR Average Hamiltonian

The nbRFDR pulse sequence is shown in Fig. 1. The basic cycle time of the nbRFDR experiment is $2N\tau_R$, during which both the isotropic and the anisotropic chemical shift interactions are refocused. An effective spin Hamiltonian for these experiments was derived by using average Hamiltonian theory (AHT) (*22*), while taking into account only isotropic chemical shifts, and by means of Floquet theory (*23*), including chemical shift anisotropy (CSA) contributions. The spin evolution is governed by the action of this Hamiltonian during the nbRFDR mixing time, $\tau_m = l \cdot 2N\tau_R$, with l an integer number. In the

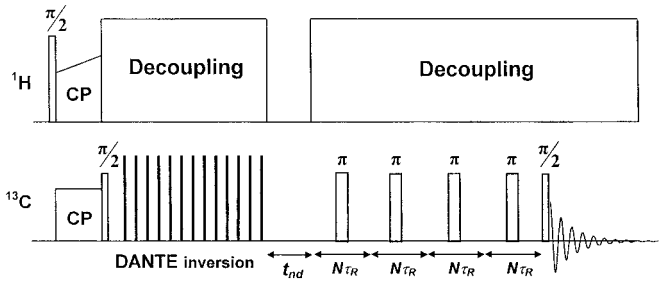

FIG. 1. The narrowband RFDR pulse sequence: An inversion of one of the spins using the DANTE sequence is followed by a delay without decoupling, t_{nd}. Then, a set of π pulses is applied, each pulse in the middle of N rotor cycles of length τ_R. A second $\pi/2$ pulse is used to transfer longitudinal magnetization into detectable signal. The standard RFDR experiment is a private case in which $N = 1$.

following, the zero-order average Hamiltonian calculation will be extended to include CSA terms. This derivation illustrates the contribution of the CSA interactions to the nbRFDR magnetization exchange mechanism. Although it resembles the Floquet derivation already presented elsewhere (*23*), the present calculation is more general and provides new insights into the physical origin of the effective dipolar interaction recovered by this pulse experiment.

The total MAS Hamiltonian of a homonuclear spin pair has the form

$$H(t) = H^1_{CS}(t) + H^2_{CS}(t) + H^{12}_D(t) + H_{RF}(t) \qquad [1]$$

with

$$H^1_{CS}(t) = \left[-\frac{1}{2}\Delta\omega + \sum_{n=-2}^{2} Z^1_n e^{in\omega_R t} \right] I^1_z$$

$$H^2_{CS}(t) = \left[+\frac{1}{2}\Delta\omega + \sum_{n=-2}^{2} Z^2_n e^{in\omega_R t} \right] I^2_z$$

$$H^{12}_D(t) = \sum_{n=-2, n\neq 0}^{2} Z^{12}_n e^{in\omega_R t} \left(2I^1_z I^2_z - \frac{1}{2}(I^1_+ I^2_- + I^1_- I^2_+) \right). \qquad [2]$$

The first two terms represent the chemical shift interactions of the two spins, and the third term represents the dipolar interaction. The isotropic chemical shifts are assumed to be equal with opposite signs, $\pm(1/2)\Delta\omega$, without loss of generality. The Z^1_n, Z^2_n are complex coefficients (*13*, *23*) that depend on the CSA anisotropy $\{\omega^1_{CSA}, \omega^2_{CSA}\}$, the asymmetry parameters $\{\eta_1, \eta_2\}$, and the Euler angles $\Omega_r = \{\alpha_r, \beta_r, \gamma_r\}$, transforming the CSA tensor of spin-1 from its principal axis system (PAS) to the rotor frame, and $\Omega_{12} = \{\alpha_{12}, \beta_{12}, \gamma_{12}\}$, transforming the PAS of the CSA tensor of spin-2 to the PAS of the CSA of spin-1. The dipolar interaction coefficients, Z^{12}_n, are proportional to the dipole–dipole coupling strength $\mu_0\gamma^2\hbar/4\pi r^3_{ij}$ and depend on the polar angles $\{\theta_d, \varphi_d\}$ of the internuclear distance vector $\vec{r}_{12}$ with respect to the PAS of spin-1 and on $\Omega_r = \{\alpha_r, \beta_r, \gamma_r\}$ (*13*). The rf Hamiltonian $H_{RF}(t)$ describes the presence of two π pulses that are applied at times $(1/2)N\tau_R$ and $(3/2)N\tau_R$, making the whole Hamiltonian periodic with a cycle time of $2N\tau_R$.

To obtain the zero-order average Hamiltonian of $H(t)$, it is convenient to transform the Hamiltonian first to the toggling frame (T) of the rf pulses and then to the interaction representation (I) of the chemical shift terms of the Hamiltonian. The chemical shift and the dipolar terms in the toggling frame, in the limit of very short π pulses, are given by

$$H^{(T)}(t) = H^{(T)}_{CS}(t) + H^{(T)}_D(t)$$

$$H^{(T)}_{CS}(t) = \begin{cases} H^1_{CS}(t) + H^2_{CS}(t) & 0 < t \leq \frac{1}{2}N\tau_R \\ -H^1_{CS}(t) - H^2_{CS}(t) & \frac{1}{2}N\tau_R < t \leq \frac{3}{2}N\tau_R \\ H^1_{CS}(t) + H^2_{CS}(t) & \frac{3}{2}N\tau_R < t < 2N\tau_R \end{cases}$$

$$H^{(T)}_D(t) = H^{12}_D(t) \quad 0 < t < 2N\tau_R. \qquad [3]$$

The dipolar term is unaffected by the pulses but does not commute with the chemical shift terms.

The interaction frame Hamiltonian consists merely of the transformed dipolar term

$$H^{(I)}(t) = \exp\left\{ i \int_0^t dt' (H^{(T)}_{CS}(t')) \right\} \times H^{12}_D(t) \exp\left\{ -i \int_0^t dt' (H^{(T)}_{CS}(t')) \right\}. \qquad [4]$$

Both transformations are cyclic in the AHT sense (*30*, *31*). The transformation to the toggling frame is cyclic because the rf Hamiltonian is periodic with $2N\tau_R$ and $\exp\{-i \int_0^{2N\tau_R} dt' H_{RF}(t')\} = 1$. The chemical shift interaction frame transformation is cyclic because the chemical shift interactions are refocused at the end of each nbRFDR cycle and $\exp\{-i \int_0^{2N\tau_R} dt' H^{(T)}_{CS}(t')\} = 1$. Therefore, calculation of the evolution operator in the original frame can be reduced to calculation of the operator in the interaction frame (*23*).

The chemical shift unitary operators can be written as a simple product of exponents

$$U_{CS}(t) = \exp\left\{ -i \int_0^t dt' (H_{CS}^1(t') + H_{CS}^2(t')) \right\}$$
$$= \exp\left\{ -i\left(\Omega_1(t) - \frac{1}{2}\Delta\omega t \right) I_z^1 \right\}$$
$$\times \exp\left\{ -i\left(\Omega_2(t) + \frac{1}{2}\Delta\omega t \right) I_z^2 \right\} \quad [5]$$

with $\Omega_i(t)$ the accumulated phases of the anisotropic chemical shift interactions,

$$\Omega_i(t) = \int_0^t dt' \sum_{n=-2}^{2} Z_n^i \exp\{in\omega_R t'\} \quad [6]$$

and

$$\Omega_i(t + N\tau_R) = \Omega_i(t). \quad [7]$$

Then it follows that

$$U_{CS}^{-1} I_z^1 I_z^2 U_{CS} = I_z^1 I_z^2$$
$$U_{CS}^{-1} I_+^1 I_-^2 U_{CS} = \exp\{i\Delta\Omega(t)\}\exp\{-i\Delta\omega t\} I_+^1 I_-^2$$
$$U_{CS}^{-1} I_-^1 I_+^2 U_{CS} = \exp\{-i\Delta\Omega(t)\}\exp\{i\Delta\omega t\} I_-^1 I_+^2 \quad [8]$$

with

$$\Delta\Omega(t) = \Omega_1(t) - \Omega_2(t)$$
$$= \int_0^t dt' \sum_{n=-2}^{2} (Z_n^1 - Z_n^2)\exp\{in\omega_R t'\}. \quad [9]$$

This difference phase is the parameter that solely represents the CSA contributions to the Hamiltonian, indicating that only the difference between the CSA tensor components affects the nbRFDR dipolar dephasing. The interaction frame Hamiltonian can now be evaluated by insertion of Eq. [8] into Eq. [4], and the result can be written as

$$H^{(1)}(t) = \sum_{n=-2}^{2} Z_n^{12} \exp\{in\omega_R t\}$$
$$\times \left(2I_z^1 I_z^2 - \frac{1}{2}(e^{i\phi(t)} I_+^1 I_-^2 + e^{-i\phi(t)} I_-^1 I_+^2) \right) \quad [10]$$

with

$$\phi(t) = \begin{cases} \Delta\Omega(t) - \Delta\omega t & \text{I} \\ 2\Delta\Omega\left(\frac{1}{2}N\tau_R\right) - \Delta\Omega(t) - \Delta\omega\cdot(N\tau_R - t) & \text{II} \\ \Delta\Omega(t) - \Delta\omega\cdot(t - 2N\tau_R) & \text{III} \end{cases}$$

$$\text{I:} \quad 0 < t < \frac{1}{2}N\tau_R$$
$$\text{II:} \quad \frac{1}{2}N\tau_R < t < \frac{3}{2}N\tau_R \ , \quad [11]$$
$$\text{III:} \quad \frac{3}{2}N\tau_R < t < 2N\tau_R$$

where the equality $\Delta\Omega(t + N\tau_R) = \Delta\Omega(t)$ has been used. In order to calculate the zero-order average Hamiltonian, we write the CSA part of the unitary operator as a sum of Fourier components:

$$\exp\{i\Delta\Omega(t)\} = \sum_{m=-\infty}^{\infty} C_m \exp\{im\omega_R t\}. \quad [12]$$

The C-coefficients define the strength of the difference between the CSA tensors. They could be considered as the MAS center and sideband amplitudes of a spin with a CSA tensor equal to this difference.

The average Hamiltonian can now be deduced by simple substitution of boundaries and integration over a whole nbRFDR cycle using the following integral:

$$\frac{1}{2N\tau_R} \int_{-N\tau_R/2}^{N\tau_R/2} \exp\{i(m+n)\omega_R t - i\Delta\omega t\} dt$$
$$= \frac{1}{2}\,\mathrm{sinc}\left\{ \frac{N\pi((m+n)\omega_R - \Delta\omega)}{\omega_R} \right\}. \quad [13]$$

The resultant zero-order average Hamiltonian is given by

$$\tilde{H}^{(0)} = -\frac{1}{2}[d^{12}(\Omega_r) I_+^1 I_-^2 + d^{12*}(\Omega_r) I_-^1 I_+^2] \quad [14]$$

with an effective dipolar frequency,

$$d^{12}(\Omega_r) = \frac{1}{2} \sum_{n=-2}^{2} \sum_{m=-\infty}^{\infty} (C_{m-n} Z_n^{12} + e^{2i\Delta\Omega(N\tau_R/2)} C_{m-n}^* Z_n^{12*})$$
$$\times \ \mathrm{sinc}\left\{ N\pi\left(m - \frac{\Delta\omega}{\omega_R} \right) \right\}. \quad [15]$$

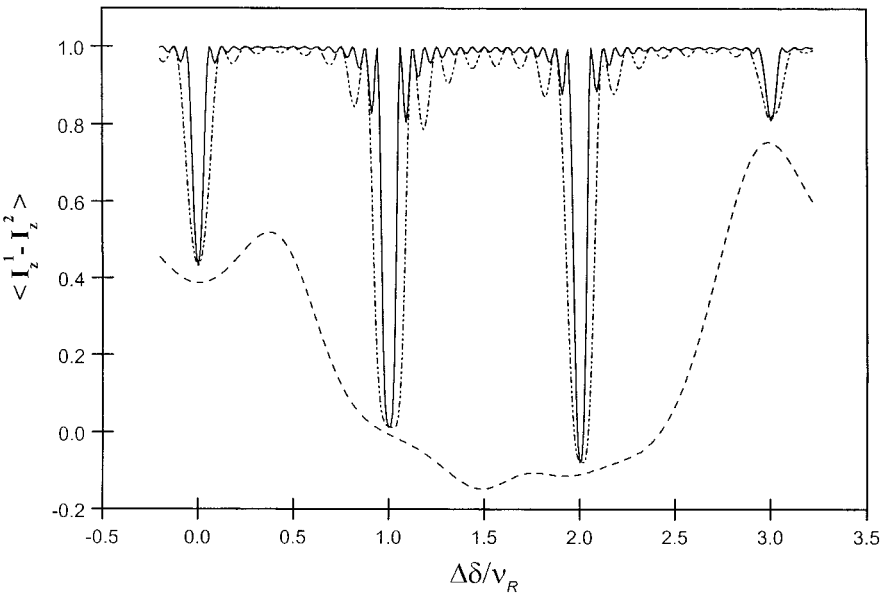

FIG. 2. Numerical calculations showing the spinning frequency dependence of the exchange between coupled spins in RFDR and nbRFDR experiments. The normalized difference signal of a coupled spin pair is plotted as a function of the isotropic chemical shift difference scaled by the spinning frequency, $\Delta\delta/\nu_R$. Simulations of nbRFDR with $N = 8$ (dash-dotted line), nbRFDR with $N = 16$ (unbroken line), and RFDR with $N = 1$ (dashed line) were carried out varying the chemical shift difference instead of the spinning frequency, for convenience. A dipolar interaction of 450 Hz, a ν_R of 10 kHz, and a mixing time of 6.4 ms were used in the simulation.

A similar expression was derived by Boender *et al.* (*24*) for even N values. The effective dipolar frequency, $d^{12}(\Omega_r)$, of a spin pair in a crystallite depends, through the dependence on the Z_n^i, Z_n^{12} coefficients, on the Euler angles $\Omega_r = \{\alpha_r, \beta_r, \gamma_r\}$. Different crystallites in a powder will, hence, experience a different effective frequency. The interaction parameters that govern the dipolar frequency are the spinning frequency, the dipolar interaction parameters, the isotropic chemical shift difference $\Delta\omega$, and the CSA tensor parameters defined by the C_m coefficients.

The dependence on the CSA parameters is very intricate and becomes significant when the spinning frequency is not much stronger than the CSA difference of the spins. The Z_n^{12} coefficients are directly proportional to the dipolar interaction strength and are used to deduce the distance between the two nuclei. As was previously derived (*6, 13*), the spin part of the Hamiltonian contains only the zero-quantum dipolar flip-flop terms $I_+^1 I_-^2$ and $I_-^1 I_+^2$. The dynamics of the spin system under such a Hamiltonian therefore takes place in the zero-quantum subspace.

In a 1D nbRFDR experiment the magnetization exchange is monitored by the time dependence of $\langle I_z^1 - I_z^2\rangle(2lN\tau_R)$,

$$\langle I_z^1 - I_z^2\rangle(2lN\tau_R) = \frac{1}{8\pi^2}\int d\Omega_r \cos\{|d^{12}(\Omega_r)|2lN\tau_R\}. \quad [16]$$

For even N values, the constant phase shift in Eq. [15] vanishes and the $d^{12}(\Omega_r)$ coefficients become real.

The sinc-function maximizes at the rotational resonance condition $\omega_R = (1/m)\Delta\omega$ and vanishes when its argument is $\pm\pi$, i.e., $\omega_R = (N/(Nm \pm 1))\Delta\omega$. Thus, the span of spinning frequencies over which the dipolar recoupling is effective around each resonance condition is approximately given by

$$\Delta\omega_R = \frac{2}{Nm^2 + m}\Delta\omega. \quad [17]$$

For RFDR ($N = 1$), the sinc-functions for different m values overlap, and a complicated exchange response as a function of the spinning frequency can be expected. For higher values of N, the sinc-functions become narrow, and efficient magnetization exchange can be expected only close to the rotational resonance conditions. The efficacy of the nbRFDR recoupling is shown in Fig. 2 as the normalized residual signal plotted vs the chemical shift difference scaled by the spinning frequency. The reciprocal dependence of the bandwidth on N causes the experiment to become more frequency selective at higher values of N. Without any significant overlap of the sinc-functions, the value of $d^{12}(\Omega_r)$ at the R^2 conditions becomes independent of N (for even N),

$$d^{12}(\Omega_r) = \sum_{n=-2}^{2}\sum_{m=-\infty}^{\infty} \mathrm{Re}\{C_{m-n}Z_n^{12}\}. \quad [18]$$

This result can be compared to the dipolar coefficient in an R^2 experiment,

$$d^{12}_{R^2}(\Omega_r) = \sum_{n=-2}^{2} \sum_{m=-\infty}^{\infty} C_{m-n} Z^{12}_n, \qquad [19]$$

which can be deduced following a derivation similar to that above. The C-coefficients define the amplitude of the sinc-modulation. When the spinning frequency is larger than the CSA tensor strengths, these coefficients become zero, except $C_0 = 1$. This same condition is encountered when all tensor parameters of the two spins are equal. In these cases efficient nbRFDR exchange may only be expected around the R^2 conditions $m = 1, 2$. If these conditions do not hold, maximal values of $d^{12}(\Omega_r)$ are also encountered at $m = 0$ and $m > 2$. This is also shown in Fig. 2, for nbRFDR simulations using $N = 8, 16$.

The above derivation shows the complicated dependence of the dipolar coefficients on all spin parameters. For simplicity of discussion, the experimental properties of the rf pulses and higher order corrections to the average Hamiltonian were not taken into account. It is therefore preferable for the analysis of experimental nbRFDR data to measure all available CSA parameters of the two-spin system and to use a simulation program that takes into account all interaction parameters, as well as pulse parameters, and calculates the exact spin dynamics. In the following sections we show how we obtained internuclear distances using nbRFDR experiments in cases where the CSA dependence of the data is not negligible. But beforehand, we discuss the influence of broadening mechanisms on the magnetization exchange and construct a model that is then used for analysis of experimental data.

ZERO-QUANTUM AND DOUBLE-QUANTUM SPIN RELAXATION

The nbRFDR exchange between the longitudinal magnetization components of a spin pair in an individual crystallite can be described, as in the R^2 experiment (*3, 20*), by the motion of a magnetization vector $\bar{m}(\Omega_R; t)$ in the zero-quantum subspace of the spins with components

$$\begin{aligned} m_x(\Omega_r; t) &= \langle I^1_+ I^2_- + I^1_- I^2_+ \rangle(t) \\ m_y(\Omega_r; t) &= \langle I^1_+ I^2_- - I^1_- I^2_+ \rangle(t) \\ m_z(\Omega_r; t) &= \langle I^1_z - I^2_z \rangle(t). \end{aligned} \qquad [20]$$

The Hamiltonian of Eq. [14], governing the motion of this vector, has the general form

$$\bar{H} = \frac{1}{2} |d^{12}| (I^1_+ I^2_- \exp\{i\delta^{12}\} + I^1_- I^2_+ \exp\{-i\delta^{12}\}), \qquad [21]$$

with $d^{12} = |d^{12}| \exp\{i\delta^{12}\}$, and can be represented by an effective magnetic field $\bar{d}^{12}$ of strength $|d^{12}|$ in the x–y plane of the zero-quantum frame. The magnitude of this vector depends on the spinning frequency and on the selected N value of the nbRFDR experiment. During the nbRFDR mixing time the $\bar{m}(\Omega_R; t)$ vector rotates around the $\bar{d}^{12}$-field and its z-component $m_z(\Omega_r; \tau_m)$ at the end of this time, τ_m, is proportional to the difference signal, $S_1(\tau_m) - S_2(\tau_m)$, that is obtained from the signals $S_1(\tau_m) = \langle I^1_z \rangle(\tau_m)$ and $S_2(\tau_m) = \langle I^2_z \rangle(\tau_m)$ of the two nuclei. The interference of the oscillating $m_z(\Omega_r; \tau_m)$ components gives rise to a decaying signal in the powder that is equal to $S_1(\tau_m) - S_2(\tau_m) = (1/8\pi^2) \cdot \int d\Omega_r m_z(\Omega_r; \tau_m)$. This signal can be analyzed in terms of the dipolar tensor components in order to deduce the dipolar coupling strength and, from it, the internuclear distance. This analysis may require preliminary knowledge of the chemical shift parameters in the cases mentioned above.

In addition to the dipolar field, the $\bar{m}$-vectors react to a variety of other mechanisms that influence the overall powder decay. In the case of an isolated carbon spin pair, perhaps the most important effect causing additional signal attenuation, during the nbRFDR pulse experiment, is the residual interactions with the protons in the sample (*21, 22, 24*). While pulse parameters can be taken into account in numerical simulations, the effects of inefficient decoupling fields and cross-polarization during the pulses are hard to predict.

In the case of R^2 it is common to assemble the decaying effects, which are independent of the pulse parameters, as a relaxation parameter T^{ZQ}_2, influencing $\bar{m}(\Omega_r; t)$. Its magnitude has been discussed extensively in the past (*3, 20, 25, 29*), and its orientation dependence has been formalized (*26*). In most cases a single isotropic T^{ZQ}_2 relaxation time is used to reflect all mechanisms that diminish $m_x(\Omega_r, t)$ and $m_y(\Omega_r, t)$ for all Ω_r (*13, 23*). If in addition to this relaxation and the standard spin–lattice relaxation of the spins, the magnitude of $\bar{m}(\Omega_r; t)$ is reduced during the rf pulses, by cross-polarization or pulse imperfections, the effective overall relaxation mechanism in the zero-quantum subspace becomes complicated. Because only the expectation values of the diagonal elements, $\langle I^1_z \rangle$ and $\langle I^2_z \rangle$, in the spin density operator are monitored in an nbRFDR experiment, it is assumed that they decay exponentially with some time constants T^1_1 and T^2_1, respectively. Furthermore, it is assumed that these relaxation mechanisms change the effective zero-quantum relaxation time, T^{ZQ}_2, by some unknown amount. A rigorous analysis of the spin evolution requires a spin density calculation, using the Liouville spin-operator formalism (*20, 26*). However, here we will restrict our treatment to a simple Bloch equation approach.

The spin pair evolution can then be described by the following set of rate equations, setting $\delta^{12} = 0$ in Eq. [21] for simplicity,

$$\frac{d}{dt}\begin{pmatrix} m_x \\ m_y \\ m_z \\ M_z \end{pmatrix} = \begin{pmatrix} -\Gamma^{ZQ} & 0 & 0 & 0 \\ 0 & -\Gamma^{ZQ} & d^{12} & 0 \\ 0 & -d^{12} & -\Gamma^{+} & -\Gamma^{-} \\ 0 & 0 & -\Gamma^{-} & -\Gamma^{+} \end{pmatrix}\begin{pmatrix} m_x \\ m_y \\ m_z \\ M_z \end{pmatrix}, \qquad [22]$$

introducing the z-component of a double quantum magnetization

$$\begin{aligned} M_z(\tau_m) &= \langle I_z^1\rangle(\tau_m) + \langle I_z^2\rangle(\tau_m) \\ &= S_1(\tau_m) + S_1(\tau_m) \end{aligned} \qquad [23]$$

and the relaxation parameters

$$\begin{aligned} \Gamma^{ZQ} &= \frac{1}{T_2^{ZQ}} \\ \Gamma^{+} &= \frac{1}{2}\left(\frac{1}{T_1^1} + \frac{1}{T_1^2}\right) \\ \Gamma^{-} &= \frac{1}{2}\left(\frac{1}{T_1^1} - \frac{1}{T_1^2}\right). \end{aligned} \qquad [24]$$

The general solution of these rate equations is quite complicated. However, here we only consider cases where the overall dipolar oscillations are larger than the relaxation rates, $|d^{12}| > \Gamma^{ZQ}, \Gamma^{+}, \Gamma^{-}$. The approximate solution of Eq. [22] for $m_z(\tau_m)$ and $M_z(\tau_m)$ is then

$$\begin{aligned} m_z(\tau_m) &= m_z(0)\cos d^{12}\tau_m \cdot R^{ZQ}(\tau_m) \\ M_z(\tau_m) &= M_z(0) \cdot R^{+}(\tau_m), \end{aligned} \qquad [25]$$

with $R^{+}(t) = \exp\{-\Gamma^{+}t\}$ and $R^{ZQ}(t) = \exp\{-(\Gamma^{ZQ} + \Gamma^{+})t/2\}$. As long as the dipolar frequencies are larger than the relaxation rates, the z-components of the magnetizations are independent of the difference between the individual decay processes of both spins. Moreover, when the orientation dependence of the relaxation parameters (*26*) is also neglected, the powder signals of the two spins can be written as

$$\begin{aligned} S_1(\tau_m) &= \frac{1}{2}(S_1(0) - S_2(0))\, f_d(\tau_m)\, R^{ZQ}(\tau_m) \\ &\quad + \frac{1}{2}(S_1(0) + S_2(0))\, R^{+}(\tau_m) \\ S_2(\tau_m) &= -\frac{1}{2}(S_1(0) - S_2(0))\, f_d(\tau_m)\, R^{ZQ}(\tau_m) \\ &\quad + \frac{1}{2}(S_1(0) + S_2(0))\, R^{+}(\tau_m), \end{aligned} \qquad [26]$$

where the normalized nbRFDR decay curve is defined by

$$f_d(\tau_m) = \frac{1}{8\pi^2 \cdot m_z(\Omega_r;0)} \int d\Omega_r m_z(\Omega_r;\, \tau_m), \qquad [27]$$

where $m_z\,(\Omega_r;\, 0)$ is the normalization factor of $f_d\,(\tau_m)$. These expressions cannot be used in cases where the dipolar dephasing is weak and the pulse and decoupling effects influence the signals significantly. Then this simple relaxation model is invalid and exact solution of the rate equation in Eq. [22] must be used for the analysis of the data. However, here we restrict ourselves to the approximate solution in Eq. [25] and in future work a more generalized treatment will be discussed and applied.

In the range of dipolar interactions and relaxation decay parameters, where Eq. [26] is valid, experimental nbRFDR data can be fit to simulated data based on the theoretical $f_d(\tau_m)$ functions. The powder decay signals must, therefore, be corrected by introducing two independent effective decaying functions. In practice the relaxation decay functions, $R^{ZQ}(\tau_m)$ and $R^{+}(\tau_m)$, are not necessarily simple exponential functions, and they cannot be measured easily and independently. Therefore, we suggest measuring nbRFDR exchange at variable spinning frequency, instead of measuring it as a function of the exchange time. The powder decay signals can then be measured at mixing times τ_m that change only slightly, and the data can be fitted plainly by introducing two fixed parameters $R^{ZQ}(\tau_m)$ and $R^{+}(\tau_m)$. In the next section the spinning-frequency-dependent nbRFDR approach is introduced and an experimental procedure that suits different ranges of dipolar interactions is suggested.

SPINNING-FREQUENCY-DEPENDENT nbRFDR

In nbRFDR experiments the function $f_d(\tau_m)$ strongly depends on the offset of the spinning frequency from the R^2 condition, $\Delta\omega_R = m\omega_R - \Delta\omega$, and on N. The narrowband character of these experiments makes it possible to modify the value of this function significantly by small changes to the spinning frequency. By choosing a fixed value for N and l in $\tau_m = l \cdot 2N\tau_R$ and allowing only small changes, $\pm\Delta\omega_R$, around some average ω_R, the mixing time varies by a factor approximately given by $2\Delta\omega_R/\omega_R$. If this time variation is much shorter than the relaxation times of the experiment, it is reasonable to assume that $R^{ZQ} = R^{ZQ}(\tau_m)$ and $R^{+} = R^{+}(\tau_m)$ are constant throughout the experiment. To utilize this fact, we first normalize the experimental signals $S_i(\tau_m,\, \omega_R)$, which are dependent on both the spinning frequency and the values of N and l, and define the experimental function as follows:

$$F_i(\omega_R) = \frac{S_i(\tau_m,\, \omega_R)}{(1/2)(S_i(0,\, \omega_R) - S_j(0,\, \omega_R))} \quad i, j = 1, 2. \qquad [28]$$

These functions account for the dependence of the signal on the initial state of the two spins. The signal of the inverted line will change its values from negative to positive by the action of this normalization. The mixing time τ_m is changing according to the value of the spinning frequency, but the integers N and l are kept fixed. Using Eq. [26], the nbRFDR function can now be rewritten as

$$f_{d1}(\omega_R) = c_1[F_1(\omega_R) - c_2(\omega_R)]$$
$$f_{d2}(\omega_R) = c_1[F_2(\omega_R) + c_2(\omega_R)] \qquad [29]$$

with

$$c_1 = \frac{1}{R^{ZQ}}$$
$$c_2(\omega_R) = \frac{(S_1(0, \omega_R) + S_2(0, \omega_R))}{(S_1(0, \omega_R) - S_2(0, \omega_R))} R^+. \qquad [30]$$

Two $f_{di}(\omega_R)$ functions are introduced for the two spins. They are calculated numerically and can differ slightly due to differences in the CS parameters and the effect of the pulses. The c_1 term is independent of ω_R and can be introduced as a constant parameter in data analysis. The $c_2(\omega_R)$ term is dependent on the signals at zero mixing time. In most cases we expect this term to be small, because the signal preparation is aimed at obtaining the condition $S_1(0, \omega_R) = -S_2(0, \omega_R)$. It is also expected that this term will exhibit a weak dependence on the spinning frequency caused by slight broadening as rotational resonance is approached. This dependence is simply accounted for by measuring the signal at zero mixing time. The ω_R-dependence of $f_d(\omega_R)$ is modified by particular choices of l and N. Depending on the approximate dipolar coupling, these integers must be chosen to make the measurements sensitive to small variations in the dipolar parameters.

In Figs. 3 and 4, examples of $f_d(\omega_R)$ decay curves are shown for a set of dipolar interactions, ranging from 50 to 550 Hz, corresponding to ^{13}C–^{13}C distances of 5.34 to 2.40 Å, respectively. All frequency parameters in the calculations are computed, for convenience, in units of Hz. Therefore, we redefine the isotropic chemical shift difference and the spinning frequency as $\Delta\delta = \Delta\omega/2\pi$ and $\nu_R = \omega_R/2\pi$, respectively. The $f_d(\nu_R)$ functions are calculated for $\Delta\delta = 14.6$ kHz and with zero CSA tensor parameters. Close to the $m = 1$ R^2 resonance condition, we have chosen (N, l) pairs that are equal to (16, 2) and (12, 2) for the ranges 50–350 Hz and 300–550 Hz, respectively. In the vicinity of the second $m = 2$ R^2 condition, these values are (12, 2) and (8, 2) for the same coupling ranges, respectively. As can be seen, the differences between the functions are significant and indicate that it should be possible to fit experimental $F_i(\nu_R)$ data to theoretical $f_d(\nu_R)$ functions, with the appropriate choice of c_1 and c_2 parameters, and to obtain the magnitude of the dipolar interaction.

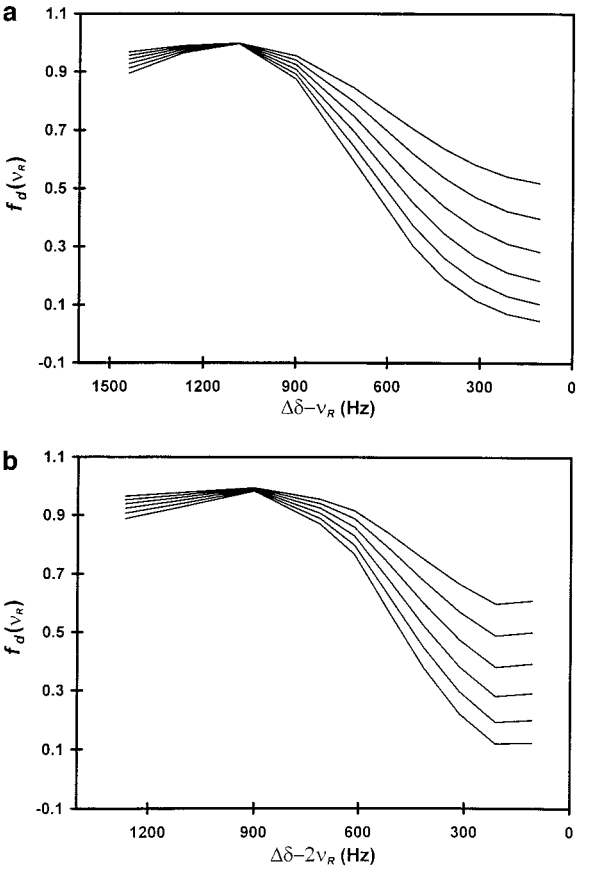

FIG. 3. Theoretical decay curves of ν_R-dependent nbRFDR experiments on a spin pair with dipolar couplings ranging between 300 and 550 Hz are plotted as a function of the proximity to the rotational resonance (R^2) conditions. In (a) calculations using an (N, l) pair of (12, 2) near the $m = 1$ R^2 condition are shown, and in (b) calculations using an (N, l) pair of (8, 2) near the $m = 2$ R^2 condition are shown. The difference between the dipolar couplings of adjacent curves in the figures is 50 Hz. The isotropic chemical shift difference used in these calculations was $\Delta\delta = 14.6$ kHz, and the CSA interactions were set to zero.

We have shown above that the $f_{di}(\nu_R)$ functions are also dependent on the CSA parameters of the coupled spins and on the direction of the dipolar vector with respect to these tensors. It is therefore necessary to take these parameters into account in data analysis. In most instances the values of the chemical shift anisotropy and asymmetry parameters can be obtained from independent measurements (*32*). However, the Euler angles transforming one CSA tensor to the other and the polar angles of the dipolar vector in one of the CSA tensor PAS frames are in general not known. The angular dependence disappears when the nbRFDR dipolar coefficients $d^{12}(\Omega_r)$ in Eq. [15] become independent of the CSA parameters. This happens when the spinning frequency is larger than the CSA interactions and the C_n-coefficients for $n \neq 0$ become negligible. The dipolar coefficients depend then only on the Z_n^{12} parameters in the spin Hamiltonian, and the data rely exclusively on the interatomic distance r_{IS}. When possible it is

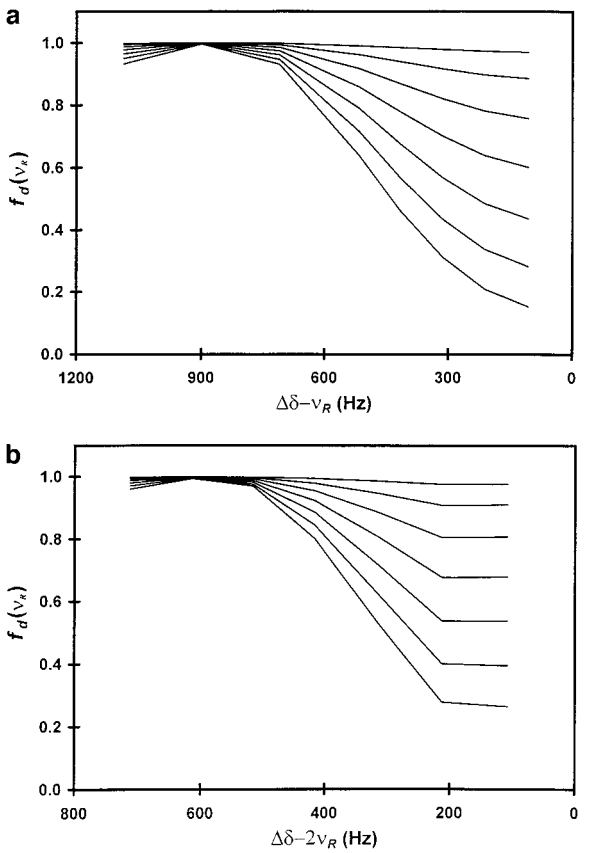

FIG. 4. Theoretical decay curves of ν_R-dependent nbRFDR experiments on a spin pair with dipolar couplings ranging between 50 and 350 Hz are plotted as a function of the proximity to the rotational resonance (R^2) conditions. In (a) calculations using an (N, l) pair of (16, 2) near the $m = 1$ R^2 condition are shown, and in (b) calculations using a (N, l) pair of (12, 2) near the R^2 $m = 2$ condition are shown. The difference between the dipolar couplings of adjacent curves in the figures is 50 Hz. The isotropic chemical shift difference used in the calculation was $\Delta\delta = 14.6$ kHz, and the CSA interactions were set to zero.

therefore advisable to perform experiments at the highest possible spinning rate, i.e., around the $m = 1$ rotational resonance condition. When for $m = 1$ the CSA effects can be neglected and the internuclear distance can be determined, additional experiments around $m = 2$, with the condition $|Z_n^1 - Z_n^2| \geq 2\omega_R$, can yield angular information.

Based on these considerations, the following experimental methodology for obtaining dipolar interactions, and from them internuclear distances by spinning-frequency-dependent nbRFDR, is proposed. For clarification we assert that we focus on the distance between two nonequivalent ^{13}C-nuclei. The following steps are suggested to implement this approach:

(i) First it is necessary to determine the isotropic chemical shifts, the CSA interactions, and the asymmetry parameters of the spins. This can be done using the Herzfeld–Berger (*32*) sideband pattern analysis of the ^{13}C MAS spectra measured by a simple off-R^2 CPMAS experiment at low spinning frequencies.

(ii) When the isotropic chemical shift difference between the spins is known, a range of spinning frequencies is chosen close to the $m = 1$ or $m = 2$ resonance condition. When possible, nbRFDR experiments around both conditions should be performed. For each m, a pair of integers N and l is chosen that satisfy $\tau_m = l \cdot 2N\tau_R$, according to the expected magnitude of the dipolar interaction, as was shown in Figs. 3 and 4.

(iii) In the next step the nbRFDR experiment is set up. After initial CPMAS excitation of the spins and a $\pi/2$ flip-back pulse, a method for selective inversion of one of the spins is chosen. The initial longitudinal magnetizations of the nbRFDR experiment are measured by setting the mixing time to zero. The initial values $S_1(0, \omega_R)$ and $S_2(0, \omega_R)$ for each spinning rate are used to correct for the broadening of the signal and changes in CP transfer efficiency as R^2 is approached. After the CPMAS excitation and the inversion, the signals are unlikely to satisfy $S_1(0, \omega_R) = -S_2(0, \omega_R)$. This condition is not crucial for the analysis of the data; however, maximizing $S_1(0, \omega_R) - S_2(0, \omega_R)$ will improve the quality of the data. At this stage two experiments are performed at a far off-R^2 spinning frequency, where no dipolar dephasing occurs; a pair (N, l) is chosen and two experiments, similar to the nbRFDR experiment, with and without pulses in the mixing time are performed. These experiments are used to render the effective relaxation parameters and enable us to ascertain the validity of Eq. [30]. If the relaxation processes cause a reduction in $S_i(\tau_m)/S_i(0)$ values that are comparable to the effective dipolar frequency, our model fails to predict the experimental results and a rigorous treatment must be undertaken to include all decaying effects in the spin dynamics simulations (*22*).

(iv) At this stage a set of nbRFDR measurements are performed as a function of the spinning rate and the signals of the two spins are acquired and normalized according to Eq. [28]. This results in two ω_R-dependent experimental functions $F_1(\omega_R)$ and $F_2(\omega_R)$.

(v) These data are analyzed in two stages. First they are shifted, according to Eq. [29]. The shift parameter $c_2(\omega_R)$ is considered constant unless the initial signals exhibit spinning frequency dependence. In that case the individual ratios of the initial signals for each spinning frequency are included in the shift procedure. A shift parameter is chosen that minimizes $\{F_1(\omega_R) - F_2(\omega_R) - 2c_2(\omega_R)\}$ and the resulting two shifted data sets $\{F_i(\omega_R) \pm c_2(\omega_R)\}$ are stored together with the average data set

$$\bar{F}(\omega_R) = (1/2)(F_1(\omega_R) + F_2(\omega_R)). \qquad [31]$$

(vi) After this procedure the shifted data sets or the resulting average data set are fitted to one of the simulated sets of functions $f_{d1}(\omega_R)$ and $f_{d2}(\omega_R)$ for different dipolar and CSA parameters. These functions are calculated taking into account all known parameters, such as spinning frequencies, isotropic

and anisotropic chemical shift parameters, (N, l) values, and pulse lengths. The fitting is ideally done using a numerical least-square procedure with two unknown parameters c_1 and d_{IS}, minimizing

$$\chi = \sum_{i=1}^{2} \sum_{j} [\, f_{di}(\omega_R^j) - c_1 \bar{F}_i(\omega_R^j)]^2, \qquad [32]$$

where the sum is over all values of the spinning frequency, ω_R^j. However, when the number of variable CSA parameters is large or the signal-to-noise ratio of the data is low, it is more efficient to fit the data by optimizing the agreement between $f_d(\omega_R)$ and $c_1\{F_i(\omega_R) \pm c_2\}$ using a proper choice of parameters in the simulation. During this minimization procedure only experimental points that corresponds to $f_{di}(\omega_R) < 1$ are considered. This ensures that the dipolar dephasing is expected to be stronger than the relaxation effect of c_1. When a good fit is achieved, the dipolar interaction strength can be extracted and from that a distance can be obtained. The accuracy of the experiment is determined by the value of χ and by the deviations between the values of $F_i(\omega_R) \pm c_2$. The whole procedure is repeated when data are obtained close to both $m = 1$ and $m = 2$ R[2] conditions. Agreement between the two experiments is, of course, required. Depending on the relative sizes of the CSA tensors, orientational information can also be obtained.

(vii) By writing the expressions for the signals of the two spins separately, the determination of distances between a fully labeled spin and a natural abundant spin could also be accomplished when the isotope abundances are known and the initial signals $S_i(0, \omega_R)$ are measured. Both c_1 and c_2 parameters must then be determined during the fitting procedure. This approach is under investigation at the moment.

MATERIALS AND EXPERIMENTAL METHODS

DL-3-Hydroxybutyric acid (HBA) 1,3-$^{13}C_2$ sodium salt was purchased from Isotec Inc., Matheson, USA. Experiments on the HBA sample were carried out on a Bruker 300DSX spectrometer equipped with a 4-mm WB MAS probe tuned to ^{1}H and ^{13}C frequencies. Continuous wave decoupling was applied during preparation and mixing periods with an rf power of 92.5 kHz, and TPPM decoupling was applied in the acquisition period with the same rf power. Cross polarization to carbons was achieved using a ^{13}C rf power of 65 kHz. The DANTE inversion employed 32 pulses of 0.35 μs (5°) at a power level of 60 kHz. The total DANTE time was adjusted to be an integer multiple of τ_R. The nondecoupled period was set to 9 ms to remove residual transverse magnetization. Preparation and detection $\pi/2$ pulses were applied at an rf power of 90 kHz. Experiments near the $m = 1$ condition were performed at spinning frequencies of 7800 to 8500 Hz stabilized within ± 1 Hz.

TABLE 1
Chemical Shift Anisotropy Values of the Hydroxyl and Carboxyl Carbons in 3-Hydroxybutyric Acid (HBA)

	δ_{iso}	δ_{11}	δ_{22}	δ_{33}
C–OH$^{(1)}$	62.0	4.4	27.7	−32.1
C–OH$^{(2)}$	65.5	7.8	24.1	−31.9
COOH	180.5	17.8	61.4	−79.2

Note. All values are given in units of ppm, averaged from CPMAS measurements at spinning frequencies of 0.6, 2.0, and 2.5 kHz.

Mixing π pulses of 30 and 90 kHz were used in two separate experiments. Experiments near the $m = 2$ condition were performed at spinning frequencies of 4444 to 4800 Hz stabilized within ± 1 Hz. Mixing π pulses of 90 kHz were used in these experiments. The pulses were phase cycled according to the XY-4 phase cycle (*34*).

All simulations were carried out using the K4 (*35*) spin dynamics program and the SIMPSON simulation package for solid-state NMR (*36*) that take into account CSA parameters and angles, dipolar coupling and polar angles, isotropic shifts, and finite length pulses. Chemical shift anisotropy parameters of the hydroxyl and COOH carbons in HBA are summarized in Table 1. They were deduced from the sideband pattern of slow-spinning CPMAS experiments using the Bruker Xedplot software. This program is based on the Herfeld–Berger procedure for extraction of CSA values from the sideband manifold.

RESULTS AND DISCUSSION

NbRFDR measurements were carried out on a doubly ^{13}C-labeled sample of 3-hydroxybutyric acid (HBA), shown in Fig. 5. The HBA molecule is labeled at the hydroxyl and carboxyl carbons. The crystal structure of this compound is not available; however, the structure of an HBA derivative, where the methyl hydrogens are replaced by chlorine atoms, namely, 4,4,4-trichloro-3-hydroxybutyric acid (Cl-HBA), has been determined (*33*). The distance between the hydroxyl and carboxyl carbons in this derivative is 2.48 Å. Assuming that the molecular structure of the hydroxybutyric acid is the same in the two compounds, we expect to measure a similar distance, corresponding to a dipolar interaction of 485 Hz. The carbon MAS NMR spectrum of the enriched HBA sample consists of three dominant peaks. The carboxyl carbon has an isotropic chemical shift of 180.5 ppm and the hydroxyl carbon shows two well-resolved resonances at 62.0 ppm and 64.6 ppm. The more shielded hydroxyl resonance is denoted by C–OH$^{(1)}$ and the less shielded one by C–OH$^{(2)}$. The isotropic shift differences between the carboxyl line and the two hydroxyl lines are $\Delta\delta^{(1)} = 118.5$ ppm and $\Delta\delta^{(2)} = 115.9$ ppm, respectively, corresponding to 8933 and 8747 Hz on our 300-MHz spectrometer. The CSA parameters corresponding to the three lines

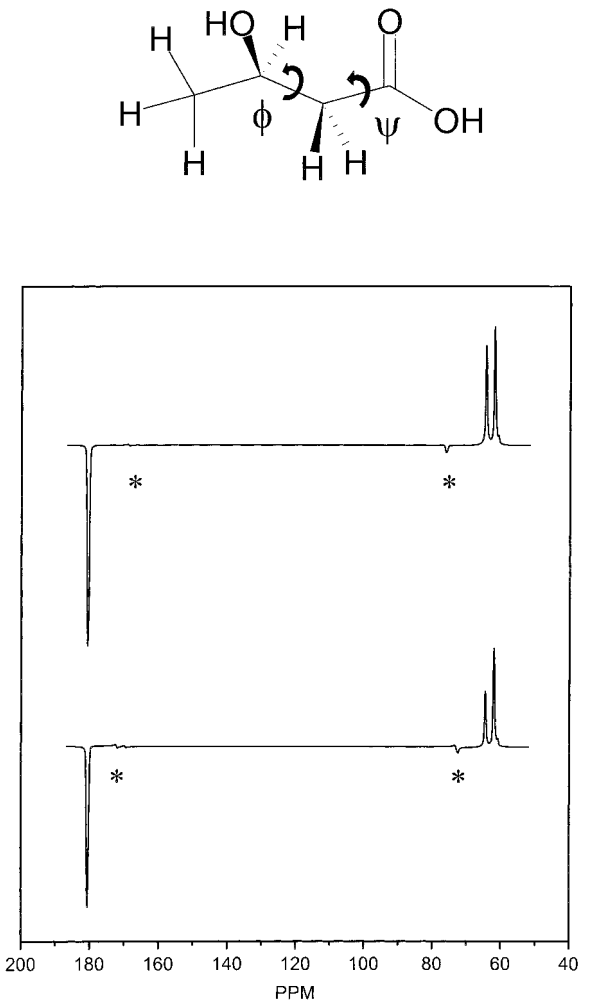

FIG. 5. The 3-hydroxybutyric acid (HBA) molecule is drawn together with ^{13}C nbRFDR spectra of a doubly ^{13}C-labeled HBA sample. The COOH sideband at ~70 ppm and the C–OH$^{(1)}$ and C–OH$^{(2)}$ sidebands at ~170 ppm are marked with stars. Spectrum (a) was recorded at a ν_R of 7874 Hz, corresponding to $\Delta\delta^{(2)} - \nu_R = 870$ Hz of the C–OH$^{(2)}$ line and $\Delta\delta^{(1)} - \nu_R = 1060$ Hz of the C–OH^1 line. Spectrum (b) was recorded at a ν_R of 8130 Hz, corresponding to $\Delta\delta^{(2)} - \nu_R = 620$ Hz and $\Delta\delta^{(1)} - \nu_R = 800$ Hz. A shift of the spinning frequency by 250 Hz toward the $m = 1$ R^2 condition causes an increased exchange between the carboxyl and C–OH lines and, consequently, a significant attenuation of their line intensities. In the drawing of the HBA molecule the torsion angles are indicated by round arrows.

are summarized in Table 1. The decaying signals of the carboxyl and the two hydroxyl lines were collected close to the $m = 1$ and the $m = 2$ R^2 condition, with spinning frequencies around 8100 and 4550 Hz, respectively. To demonstrate the dramatic effect of spinning frequency on the extent of dipolar exchange, the $m = 1$ nbRFDR spectrum of HBA at two adjacent spinning frequencies is plotted in Fig. 5. A shift of the spinning frequency by about 250 Hz results in substantial dipolar exchange between the COOH and C–OH$^{(2)}$ carbons and a decrease of 40% of the C–OH$^{(2)}$ line intensity for $\tau_m \cong 4$ ms and $(N, l) = (8, 2)$. The C–OH$^{(1)}$ carbon experiences a smaller effective interaction and therefore a corresponding decrease of its line intensity by only 15%.

Distance Measurements near the m = 1 Rotational Resonance

The $m = 1$ nbRFDR experiments were carried out with an (N, l) pair of (8, 2), i.e., with four π-pulses applied over 32 rotor cycles. The carboxyl line intensity is decomposed into two contributions, one experiencing coupling to the C–OH$^{(1)}$ carbon and the other to the C–OH$^{(2)}$ carbon. The experimental functions given in Eq. [28] are calculated as follows:

$$F_{\text{C–OH}(i)}(\nu_R) = \frac{S_{\text{C–OH}(i)}(\tau_m, \nu_R)}{0.5(S_{\text{C–OH}(i)}(0, \nu_R) - 0.5S_{\text{COOH}}(0, \nu_R))}$$

$$F_{\text{COOH}}(\nu_R) = \frac{0.5S_{\text{COOH}}(\tau_m, \nu_R)}{0.5(S_{\text{COOH}}(0, \nu_R) - S_{\text{C–OH}(1)}(0, \nu_R))} + \frac{0.5S_{\text{COOH}}(\tau_m, \nu_R)}{0.5(S_{\text{COOH}}(0, \nu_R) - S_{\text{C–OH}(2)}(0, \nu_R))}. \quad [33]$$

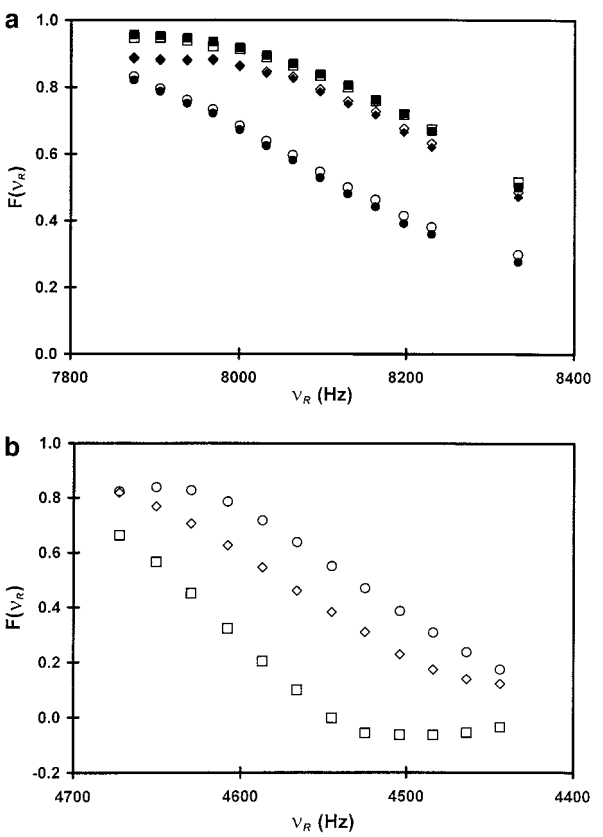

FIG. 6. The normalized experimental nbRFDR data of HBA are plotted as a function of the spinning frequency (a) close to the $m = 1$ R^2 condition and (b) close to the $m = 2$ R^2 condition. Open symbols on both plots correspond to experiments with π-pulses of 5.5 μs. The filled symbols in (a) correspond to similar nbRFDR measurements carried out with π-pulses of 16 μs. Squares, circles, and diamonds correspond to the experimental results of the C–OH$^{(1)}$, C–OH$^{(2)}$, and COOH lines, respectively.

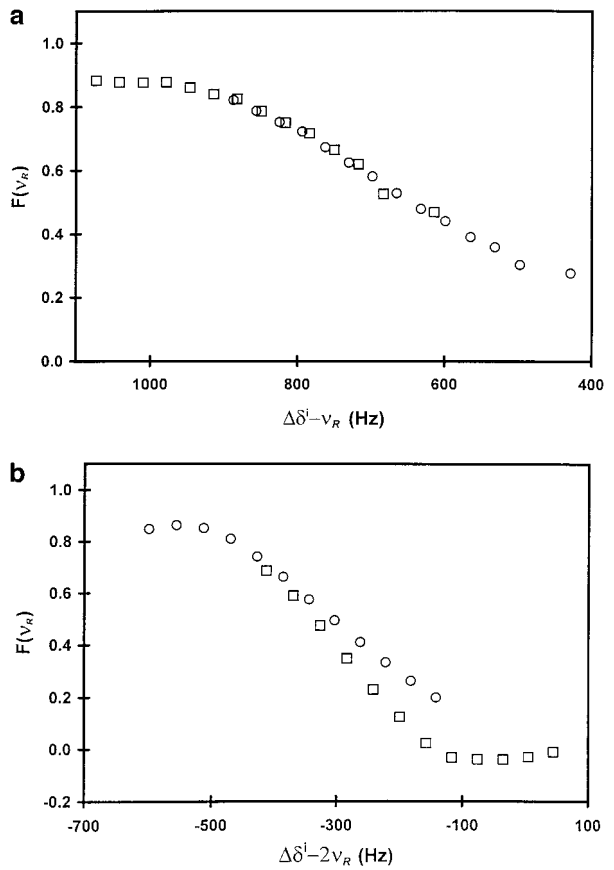

FIG. 7. The normalized experimental nbRFDR data of the C–OH$^{(1)}$ and C–OH$^{(2)}$ lines of HBA are plotted as a function of (a) $\Delta\delta^{(1)} - \nu_R$ and $\Delta\delta^{(2)} - \nu_R$ close to the $m = 1$ R^2 condition and of (b) $\Delta\delta^{(1)} - 2\nu_R$ and $\Delta\delta^{(2)} - 2\nu_R$ close to the $m = 2$ R^2 condition, respectively. The decay curves of the two hydroxyl resonances in (a) exhibit identical dipolar decay character and dissimilar dipolar decay behavior in (b).

These $F(\nu_R)$ are shown in Fig. 6a (open symbols) as a function of the spinning frequency. The spinning frequency was varied by 460 Hz, corresponding to a change of less than 6% in τ_m, between 3.84 and 4.064 ms. Similar experiments, depicted by the filled symbols in Fig. 6, were performed with 16 μs π-pulses. These experiments produced similar values for the dipolar interaction and the effective relaxation parameters. This result confirms that a carbon power as low as 30 kHz is sufficient to drive the exchange between the carbons efficiently. Experiments far off-R^2 and without nbRFDR pulses showed that the T_1 values of the ^{13}C-nuclei are larger than 400 ms, and that the pulses alone produce a signal decay of $\sim$30 msec. These time parameters are both much longer than the lengths of the nbRFDR mixing.

In Fig. 7a the experimental decay curves of the two C–OH$^{(i)}$ lines are plotted as a function of $\Delta\delta^{(i)} - \nu_R$, with $i = 1, 2$. These curves show overlapping decay curves, implying that the hydroxyl carbons associated with these resonances experience the same dipolar interaction. To obtain c_2 the average of the normalized signal intensities of the two ^{13}C–OH lines, $0.5(F_{\text{C–OH(1)}}(\nu_R) + F_{\text{C–OH(2)}}(\nu_R))$, were compared with $F_{\text{COOH}}(\nu_R)$, since the carboxyl line decays due to the exchange with both hydroxyl lines. The initial signal intensities $S(0, \omega_R)$ as a function of ω_R varied by less than 8%, justifying the use of Eq. [29] with a constant c_2 value. As a result a constant $c_2 = 0.04$ was necessary to fit the decay curves of the carboxyl and hydroxyl carbons.

The last step in the data analysis involved fitting of the shifted data of the two hydroxyl-carbons to theoretical $f_d(\nu_R)$ curves, resulting in dipolar interaction strength and a nuclear distance. In Fig. 8 the normalized and corrected nbRFDR decay curves of the C–OH$^{(1)}$ and the C–OH$^{(2)}$ carbon lines are shown. Theoretical solid curves correspond to dipolar couplings between 300 and 550 Hz. These curves were calculated ignoring the CSA parameters of the interacting carbons. Taking these CSA parameters into account resulted in shifts of the theoretical curves that were less than 6%. Thus omission of

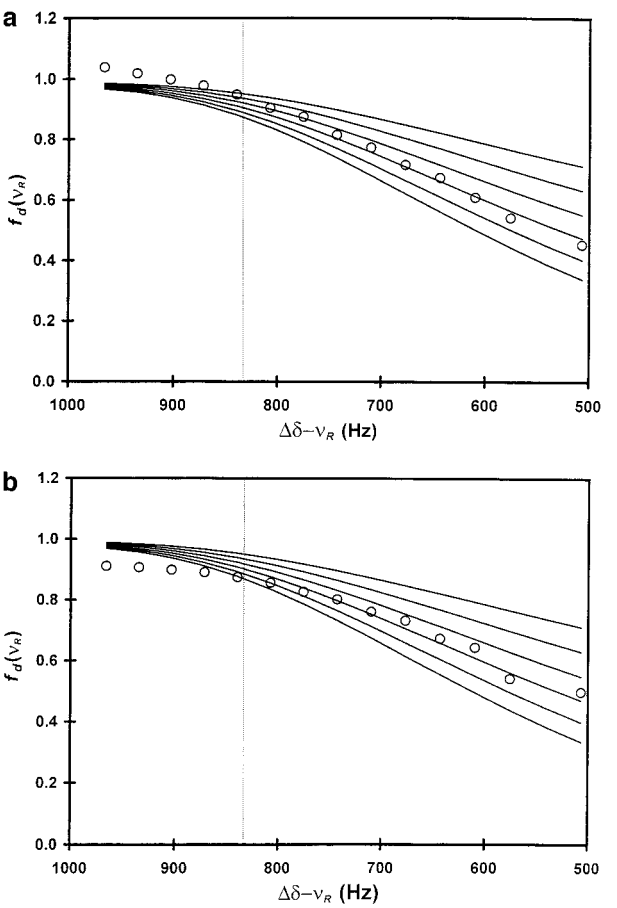

FIG. 8. The corrected experimental results (open circles) of HBA, according to Eq. [28] with $c_1 = 1.1$ and $c_2 = 0.04$, close to the $m = 1$ R^2 condition are depicted together with simulated decay curves for dipolar couplings between 300 and 550 Hz. The experimental curves of the COOH line (a) and the sum of the C–OH lines (b), as well as the theoretical lines, are plotted as a function of $\overline{\Delta\delta} - \nu_R$ with $\overline{\Delta\delta} = 0.5(\Delta\delta^{(1)} + \Delta\delta^{(2)})$. The vertical dashed lines mark the point where the theoretical model does not hold anymore and the experimental data can deviate from the relaxation-independent calculation.

CSA interactions of -2400 and -6000 Hz is justified for spinning frequencies ranging between 7800 and 8500 Hz. Good agreement with one of the theoretical curves is obtained for a value of $c_1 = 1.1$. For both carbons the dipolar coupling of the best fit was 450 ± 50 Hz, corresponding to an internuclear distance of 2.5 ± 0.1 Å. This distance is thus comparable to the reported result for the Cl-HBA derivative (*33*). The value of 1.1 for the c_1-parameter corresponds to an effective ZQ relaxation time of about 40 ms. This is of the same order of magnitude as the effective relaxation parameter of 30 ms measured above. At spinning frequencies corresponding to $|\Delta\delta - \nu_R|$ values that are larger than 800 Hz, the effective dipolar frequency becomes smaller than 30 Hz. In this region the simplified relaxation model is no longer valid and we must not expect an agreement between theory and experiments. In Fig. 8 this boundary value is represented by the vertical dotted line, indicating the positions where the deviations between experimental and calculated data become significant.

CSA Orientation by Measurements near $m = 2$ Rotational Resonance

NbRFDR experiments on HBA were repeated close to the $m = 2$ R^2 condition with (N, l) values equal to (8, 2). The normalized $F(\nu_R)$ curves of the three carbon lines, shown in Fig. 6b, were again computed from the experimental carbon signals as a function of the spinning frequency and for $\tau_m = 0$, as given in Eq. [33]. The dipolar decays of the two hydroxyl resonances are replotted in Fig. 7b as a function of their $\Delta\delta^{(i)} - 2\nu_R$ values. As can immediately be seen from these results, the two hydroxyl lines do not follow the same dipolar decay function and therefore do not experience the same effective dipolar interaction. The divergence of the two functions can not stem from a difference between the carbon distances COOH $\leftrightarrow$ C–OH$^{(1)}$ and COOH $\leftrightarrow$ C–OH$^{(2)}$, since the $m = 1$ nbRFDR measurements indicated that they are equal. We must therefore conclude that in the $m = 2$ nbRFDR experiments, the CSA tensor parameters influence the dipolar decay substantially. Additionally, the large deviation between the two data sets in Fig. 7b can not be resolved by taking into account the small differences in the principal values of the CSA tensors of the two hydroxyl carbons. Thus it must be a result of the presence of two types of HBA molecules in the sample having two unique conformations. Since the carboxyl carbons exhibit a single line in the carbon spectrum and the hydroxyl carbon two lines, we expect that the NMR data can be explained by a change in the relative orientation of the hydroxyl moiety in the molecule. As discussed in the theoretical section the dipolar decay curves of two interacting carbons are indeed dependent, besides the dipolar coupling strength, the isotropic chemical shift difference, and the rf pulse parameters, on the difference between the CSA tensors. Their principal values are determined experimentally, but the directions of the principal axes are not known. Thus the data must be compared to simulated decay curves for different relative CSA tensor orientations.

The structure of the HBA molecule can be defined by two torsion angles around carbon–carbon bond directions, assuming that the bond lengths and angles are fixed and the methyl group performs a fast threefold jump motion. The two torsion angles that can affect the relative orientation of the hydroxyl and carboxyl CSA tensors are

ψ, the torsion angle of the methine–hydroxyl carbon bond around the carboxyl–methine carbon bond, and

ϕ, the torsion angle of the bond between the carbon and the oxygen of the hydroxyl group around the methine–hydroxyl carbon bond.

To investigate the ψ- and ϕ-dependence of the nbRFDR decay functions, we assume that the structural parameters of the protons, oxygens, and carbons in HBA and in its derivative Cl-HBA are the same. These parameters are known (*33*) and are assigned to the $\psi = \phi = 0$ conformation of HBA.

To continue we must determine the CSA tensor directions with respect to the local structure of the carboxyl and hydroxyl carbons. Examples of the relative directions of the principal axes of these CSA tensors can be found in the literature, and we have chosen tensor orientations that are about consistent with reported directions (*37–39*). In the case of the carboxyl carbon, the tensor was fixed with its σ_{zz}-axis perpendicular to the sp^2 plane and the σ_{yy}-axis in the direction of the methine–carboxyl bond. The CSA tensor of the hydroxyl carbon was oriented with its σ_{zz} in the direction of the C–OH bond and σ_{yy} perpendicular to the plane defined by the methyl–hydroxyl bond and the C–OH bond. The directions of these tensor components are of course not exact, but we expect that they do not deviate significantly ($\pm 15°$) with respect to their real directions (*37–39*). The relative orientations of these tensors are expressed by the Euler angles $\Omega_{12} = \{\alpha_{12}, \beta_{12}, \gamma_{12}\}$ defining the transformation of a vector in the PAS of the hydroxyl CSA to the PAS of the carboxyl CSA. Calculating these Euler angles for $\psi = \phi = 0$, while using the atomic coordinates of Cl-HBA in Ref. (*33*), gave the values (220, 167, 305). The polar angles (θ_D, φ_D) of the carboxyl–hydroxyl carbon–carbon vector in the PAS of the carboxyl carbon were also computed for $\psi = \phi = 0$ and resulted in (102, 124). For each pair of torsion angles we calculated the corresponding Ω_{12} and (θ_D, φ_D) angles and the expected nbRFDR decay curve $f_d(\nu_R)$ for a C–OH line as a function of the off-R^2 value, $(\Delta\delta - 2\nu_R)$, taking into the account the experimental (N, l) values. In addition, a contour plot of the value of $f_d(\nu_R)$ for a fixed spinning frequency, 4587 Hz, as a function of the ψ and ϕ has been constructed and is shown in Fig. 9. Because the σ_{yy}-axis of the carboxyl CSA tensor is aligned along the ψ rotation axis, only half of the contour plot between $0 \leq \psi < 180$ is shown. The experimental values of $f_d(\nu_R)$ for the C–OH$^{(1)}$ and C–OH$^{(2)}$ carbons are 0.19 and 0.38, respectively. These values do not correspond to a unique pair of angles (ψ, ϕ). We therefore compared the $f_d(\nu_R)$ curve for the torsion angles $(\psi, \phi) = (0, 0)$ with the experimental data and found that the data $F_d^{(1)}(\nu_R)$ of C–OH$^{(1)}$ are

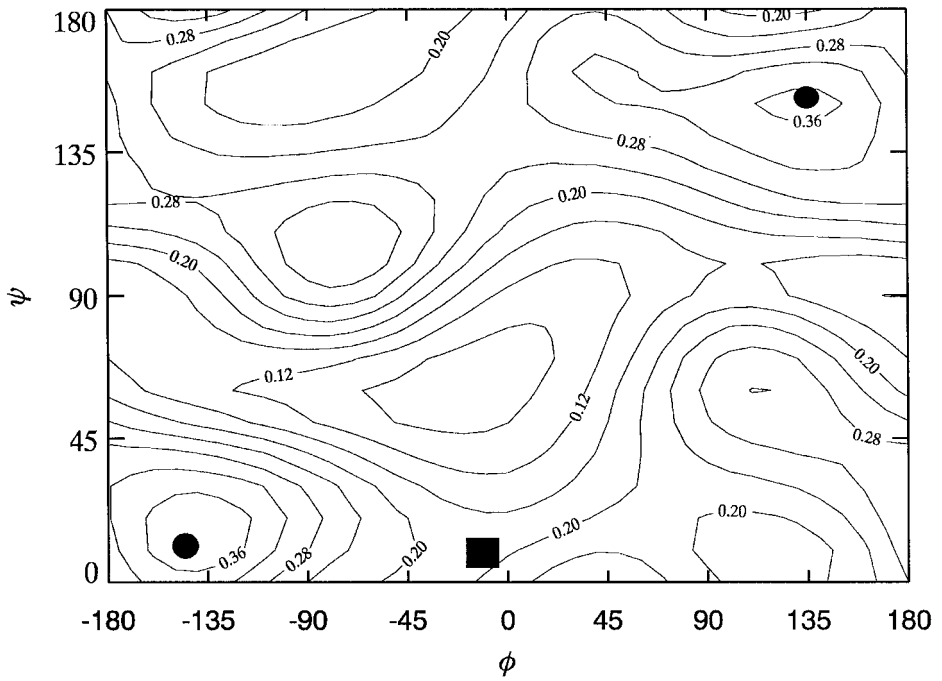

FIG. 9. Contour plot showing the calculated decay of hydroxyl carbons in HBA at a spinning frequency of 4587 Hz, as a function of the torsion angles ψ and ϕ. On a $\Delta\delta^{(i)} - 2\nu_R$ scale, this spinning frequency corresponds to an off-R^2 value of -425 Hz for the C–OH$^{(1)}$ carbon and -241 Hz for the C–OH$^{(2)}$ carbon. Contour levels increase in units of 0.04. Experimental results for the C–OH$^{(2)}$ carbon, depicted by a filled circle, and for the C–OH$^{(1)}$ carbon, depicted by a filled rectangle, are overlaid on the plot. The C–OH$^{(2)}$ molecule can reside in either a (105, -75) conformation or a (140, 150) conformation. The C–OH$^{(1)}$ molecule can be in many possible conformations; however, its experimental value is marked at the (15, -15) conformation which is closest to the crystal structure conformation of Cl-HBA.

very close to this curve. A best fit close to this zero torsion angles resulted in a set of angles in the range (15 ± 15, -15 ± 30). The spread of this range of possible angles is due to the insensitivity of $f_d(\nu_R)$ to changes in (ψ, ϕ) in the neighborhood of (0, 0). The result of this fitting procedure is shown in Fig. 10a. It conforms to the structural assumption and shows that only C–OH$^{(2)}$ satisfies the Cl-HBA conformation. The fitting of the C–OH$^{(1)}$ data is shown in Fig. 10b and corresponds to a set of torsion angles (15 ± 5, -140 ± 15). Other pairs of angles, which have nbRFDR curves close to the curve of this pair, are located on the contour plot at (105, -75) and (140, 150). Plotting the complete decay curves for these conformations as a function of the spinning frequency and comparing them with $F_d^{(2)}(\nu_R)$ showed that the (105, -75) conformation can be rejected. The remaining angles are possible, but it is more likely that the first pair describes the data. The main difference between the conformations of C–OH$^{(1)}$ and C–OH$^{(2)}$ in the HBA molecules corresponds then to a rotation of the hydroxyl carbon around the methine–hydroxyl carbon bond of about $-120°$. This rotation interchanges the proton, methyl, and hydroxyl bond directions in C–OH$^{(1)}$ with those in C–OH$^{(2)}$.

CONCLUSIONS

We have shown that spinning-frequency-dependent nbRFDR experiments provide an alternative method for measuring confined structural features of homonuclear spin pairs. It can be used at high magnetic fields, employs a small number of π-pulses, and does not require strong rf fields. It has the frequency selectivity of RFDR and can be used to monitor specific interacting spin pairs (*22*, *23*). The nbRFDR results are influenced by relaxation mechanisms in a fashion similar to other recoupling techniques (*7*, *24*). A simple relaxation model that includes contributions from zero-quantum relaxation phenomena, spin–lattice relaxation times, and pulse imperfections has been suggested. Because in our experiments the lengths of the dipolar mixing times are about constant, the effects of relaxation processes, which are slower than the dipolar dephasing, can be conveniently eliminated by simple data manipulation.

The nbRFDR approach is demonstrated on a doubly labeled HBA, setting up a methodology and displaying the differences that can be expected for $m = \pm 1$ and $m = \pm 2$ R^2 conditions. In our case the first R^2 condition provided a nuclear distance and the second R^2 condition supplied us with relative orientations of the CSA tensors and molecular conformations.

Applying the spinning-dependent nbRFDR approach for measuring large distances between ^{13}C nuclei could require a modification of the simple relaxation model for the data analysis. Exact solutions of the rate equation in Eq. [22] and the introduction of orientational dependent relaxation parameters could be necessary when the dipolar interactions become of the

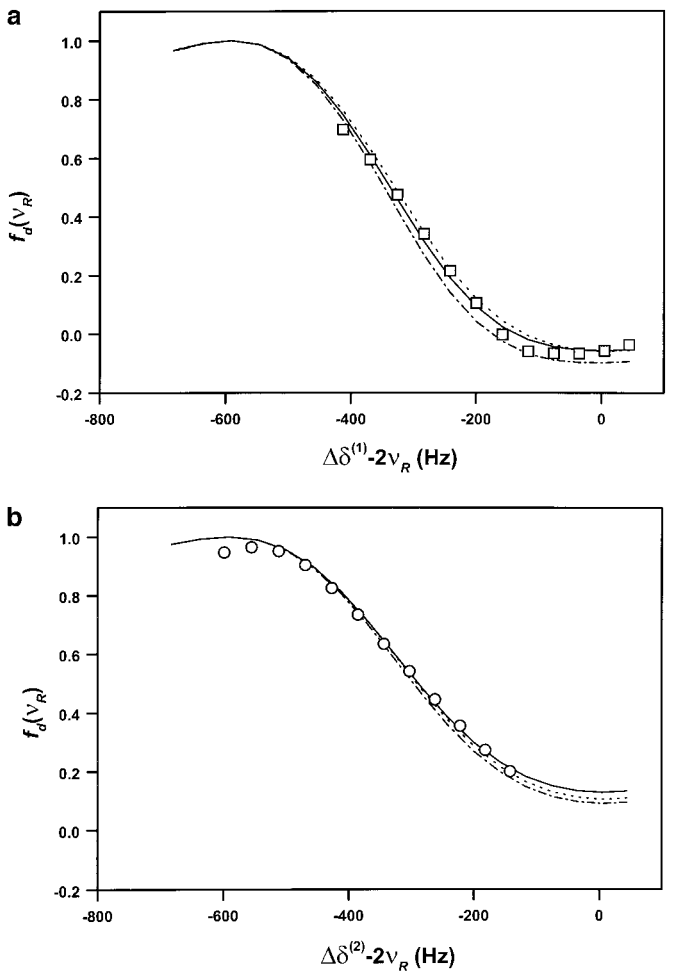

FIG. 10. The corrected nbRFDR experimental results (open symbols) of HBA are plotted with simulated curves of several ψ and ϕ values. The best-fit simulated curves are shown as a solid line in the two graphs and correspond to (ψ, ϕ) values of (15, −140) for C–OH$^{(1)}$ (a) and (15, −15) for C–OH$^{(2)}$ (b). Simulations of neighboring conformations are shown as dotted and dash-dotted curves. In (a), the dash-dotted curve corresponds to a simulated decay of a (20, −140) conformation and the dotted line corresponds to a (15, −125) conformation. In (b), the dash-dotted curve corresponds to a simulated decay of a (30, −15) conformation and the dotted line corresponds to a (15, −60) conformation. Signal-to-noise ratios in all nbRFDR and reference experiments are larger than 100; therefore, error ranges in the torsion angles, stated in the text, were deduced only by the spread of the experimental points around the simulated curves.

same order of magnitude as the relaxation rates. Also, when the isotropic chemical shift differences become much smaller than the magnitudes of the CSA tensors or the values of the spinning frequencies at the R^2 conditions become small, modifications in the analysis of nbRFDR data must be considered. Narrowband RFDR experiments on singly ^{13}C-labeled samples can also be performed, provided spectra with sufficient dynamic range can be achieved. All these issues must be investigated and methodologies must be developed to extend the applicability of the spinning-frequency-dependent one-dimensional nbRFDR experiments.

ACKNOWLEDGMENTS

The authors thank Mads Bak and Niels C. Nielsen for providing us with the SIMPSON spin dynamics program. This research was supported by the German-Israeli foundation.

REFERENCES

1. M. E. Stoll, A. J. Vega, and R. W. Vaughan, *J. Chem. Phys.* **65,** 4093–4098 (1976); R. A. Haberkorn, R. E. Stark, H. van Willigen, and R. G. Griffin, *J. Am. Chem. Soc.* **103,** 2534–2539 (1981).
2. T. Gullion and J. Schaefer, *Adv. Magn. Reson.* **13,** 57–83 (1989).
3. M. H. Levitt, D. P. Raleigh, F. Creuzet, and R. G. Griffin, *J. Chem. Phys.* **92,** 6347–6364 (1990).
4. R. Tycko and G. Dabbagh, *Chem. Phys. Lett.* **173,** 461–465 (1990).
5. T. Gullion and S. Vega, *Chem. Phys. Lett.* **194,** 423–428 (1992).
6. A. E. Bennett, J. H. Ok, R. G. Griffin, and S. Vega, *J. Chem. Phys.* **96**(11), 8624–8627 (1992).
7. D. K. Sodickson, M. H. Levitt, S. Vega, and R. G. Griffin, *J. Chem. Phys.* **98**(9), 6742–6748 (1993).
8. T. Fujiwara, A. Ramamoorthy, K. Nagayama, K. Hioka, and T. Fujito, *Chem. Phys. Lett.* **212,** 81–84 (1993).
9. M. Baldus, M. Tomaselli, B. H. Meier, and R. R. Ernst, *Chem. Phys. Lett.* **230,** 329–336 (1994).
10. B. Q. Sun, P. R. Costa, D. A. Kocisko, P. T. Lansbury, Jr., and R. G. Griffin, *J. Chem. Phys.* **102,** 702–707 (1995).
11. D. M. Gregory, D. J. Mitchell, J. A. Stringer, S. Kiihne, J. C. Shiels, J. Callahan, M. A. Mehta, and G. P. Drobny, *Chem. Phys. Lett.* **246,** 654–663 (1995).
12. Y. K. Lee, N. D. Kurur, M. Helmle, O. G. Johannessen, N. C. Nielsen, and M. H. Levitt, *Chem. Phys. Lett.* **242,** 304–309 (1995); M. Hohwy, C. M. Rienstra, C. P. Jaroniec, and R. G. Griffin, *J. Chem. Phys.* **110,** 7983–7992 (1999).
13. A. E. Bennett, R. G. Griffin, and S. Vega, *NMR Basic Princ. Progr.* **33,** 1–77 (1994).
14. J. Schaefer and E. O. Stejskal, *J. Am. Chem. Soc.* **98,** 1031–1032 (1976).
15. M. Maricq and J. S. Waugh, *J. Chem. Phys.* **70,** 3300–3315 (1979).
16. E. R. Andrew, A. Bradbury, R. G. Eades, and V. T. Wynn, *Phys. Lett.* **4,** 99–101 (1963); D. P. Raleigh, S. G. Harbison, T. G. Neiss, J. E. Roberts, and R. G. Griffin, *Chem. Phys. Lett.* **138,** 285–290 (1987); B. H. Meier and W. L. Earl, *J. Am. Chem. Soc.* **109,** 7937–7941 (1987).
17. D. P. Raleigh, F. Creuzet, S. K. Das Gupta, M. H. Levitt, and R. G. Griffin, *J. Am. Chem. Soc.* **111,** 4502–4503 (1989).
18. J. R. Garbow and T. Gullion, *in* "Carbon 13 NMR Spectroscopy of Biological Systems" (N. Beckmen, Ed.), pp. 65–115, Academic Press, San Diego (1995); S. O. Smith, K. Aschheim and M. Groesbeek, *Q. Rev. Biophys.* **29,** 395–449 (1996); B. Bechinger, R. Kinder, M. Helmle, T. C. B. Vogt, U. Harzer, and S. Schinzel, *Biopolymers* **51,** 174–190 (1999); X. Feng, P. J. E. Verdegem, Y. K. Lee, M. Helmle, S. C. Shekar, H. J. M. de Groot, J. Lugtenburg, and M. H. Levitt, *Solid State Nucl. Magn. Reson.* **14**(2), 81–90 (1999).
19. M. G. Colombo, B. H. Meier, and R. R. Ernst, *Chem. Phys. Lett.* **146,** 189–196 (1988); A. Kubo and C. A. McDowell, *J. Chem. Soc. Faraday Trans.* **84,** 3713–3730 (1988).
20. T. Karlsson and M. H. Levitt, *J. Chem. Phys.* **109**(13), 5493–5507 (1998).
21. A. E. Bennet, D. P. Weliky, and R. Tycko, *J. Am. Chem. Soc.* **120,** 4897–4898 (1998).

22. A. E. Bennett, C. M. Rienstra, J. M. Griffiths, W. Zhen, P. T. Lansbury, Jr., and R. G. Griffin, *J. Chem. Phys.* **108**(22), 9463–9479 (1998).

23. G. J. Boender, Ph.D. Thesis, Leiden Univ., The Netherlands, 1996; G. J. Boender, S. Vega, and H. J. M. de Groot, *J. Chem. Phys.* **112,** 1096–1106 (2000).

24. P. R. Costa, B. Sun, and R. G. Griffin, *J. Am. Chem. Soc.* **119,** 10821–10830 (1997).

25. A. Kubo and C. A. McDowell, *J. Chem. Soc. Faraday Trans.* **84,** 3713–3730 (1988).

26. M. Helmle, Y. K. Lee, P. J. E. Verdegem, X. Feng, T. Karlsson, J. Lugtenburg, H. J. M. de Groot, and M. H. Levitt, *J. Magn. Reson.* **140**(2), 379–403 (1999).

27. Y. S. Balazs and L. K. Thompson, *J. Magn. Reson.* **139,** 371–376 (1999).

28. G. J. Boender, J. Raap, S. Prytulla, H. Oschkinat, and H. J. M. de Groot, *Chem. Phys. Lett.* **237,** 502–508 (1995).

29. S. R. Kiihne, K. B. Geahigan, N. A. Oyler, H. Zebroski, M. A. Mehta, and G. P. Drobny, *J. Phys. Chem. A* **103,** 3890–3903 (1999).

30. U. Haeberlen, "High Resolution NMR in Solids: Selective Averaging," Suppl. 1 Adv. Magn. Reson., Academic Press, New York (1976).

31. R. R. Ernst, G. Bodenhausen, and A. Wokaun, "Principles of Nuclear Magnetic Resonance in One and Two Dimensions," Clarendon, Oxford (1987).

32. J. Herzfeld and E. Berger, *J. Chem. Phys.* **73,** 6021–6030 (1980); T. M. de Swiet, *J. Chem. Phys.* **110,** 5231–5237 (1999).

33. L. A. Aslanov, V. M. Ionov, V. A. Tafeenko, and A. N. Kost, *Zh. Strukt. Khim.* **17,** 748–749 (1976).

34. T. Gullion, D. B. Baker, and M. S. Conradi, *J. Magn. Reson.* **89,** 479–484 (1990).

35. S. M. Holl, G. R. Marshall, D. D. Beusen, K. Kociolek, A. S. Redlinski, M. T. Leplawy, R. A. Mckay, S. Vega, and J. Schaefer, *J. Am. Chem. Soc.* **114,** 4830–4833 (1992).

36. M. Bak, J. T. Rasmussen, and N. C. Nielsen, 40th Experimental NMR Conference, Monday and Tuesday poster number 198, Orlando, FL, 1999.

37. N. Janes, S. Ganapathy, and E. Oldfield, *J. Magn. Reson.* **54,** 111–121 (1983).

38. W. S. Veeman, *Prog. NMR Spectrosc.* **16,** 193–235 (1984).

39. CH. Ye, RQ. Fu, JZ. Hu, L. Hou, and S. W. Ding, *Magn. Reson. Chem.* **31,** 699–704 (1993).